A highly accurate beam finite element for curved and twisted helicopter blades

Yan Skladanek, Paul Cranga, Guy Ferraris, Georges Jacquet Richardet, Régis Dufour

**Proceedings of the ASME 2011 International Design Engineering Technical Conferences &
Computers and Information in Engineering Conference
IDETC/CIE 2011
August 28-31, 2011, Washington, DC, USA**

DETC2011-47055

A HIGHLY ACCURATE BEAM FINITE ELEMENT FOR CURVED AND TWISTED HELICOPTER BLADES

Yan Skladanek*
EUROCOPTER-Dynamics Department
F-13725 Marignane Cedex, France
Université de Lyon, CNRS, INSA-Lyon
LaMCoS UMR5259
F-69621, Villeurbanne, France
Email: yan.skladanek@eurocopter.com

Paul Cranga
EUROCOPTER
Dynamics Department
F-13725 Marignane Cedex, France

**Guy Ferraris,
Georges Jacquet, Régis Dufour**
Université de Lyon, CNRS, INSA-Lyon
LaMCoS UMR5259
F-69621, Villeurbanne, France

ABSTRACT

Blade optimization is more than ever a crucial activity for helicopter manufacturers, always looking for performance improvements, noise reduction and vibratory comfort increase. Latest studies have led to design new blade concepts including a double swept plan shape, an evolutionary and increased twist angle at the tip and a new layout for internal components like roving spars. Such blades exhibit a highly coupled behavior between torsion, longitudinal and bending motions that should be accurately modeled for predictive numerical tools. In this research a highly accurate beam finite element is formulated in the rotating frame to improve the static deformation calculation under aerodynamic and centrifugal loads and thus enhance dynamic and stability analysis usually performed for a helicopter development. Numerical and experimental investigations are performed to demonstrate the model reliability both for academic beams with extreme shape and for actual blade design.

NOMENCLATURE

BAM Beam Advanced Model.
DoF Degree of Freedom.
FE Finite Element.
InP In Plane.
OuP Out of Plane.
SdB Standard Beam.

$a_{\xi,\eta}$	Shear coefficients.
$C_{\xi,\eta}$	Additional shear angles.
E	Young modulus.
G	Shear modulus.
J_T	Torsion constant.
$k_{\xi,\eta}$	Timoshenko's shear coefficients.
L	Beam length.
q, q_i	Generalized coordinates.
T	Kinetic energy.
U	Strain Energy.
ε	Strain.
θ	Twist angle.
ρ	Density.
σ	Stress.
ϕ	Torsion angle.
$\phi_{\xi,\eta}$	Bending angles.
Ω	Speed of rotation.
$\dot{()}$	Derivative of time $\partial/\partial t$.
$()'$	Derivative of space $\partial/\partial x$.
$\langle\ \rangle$	Row vector.
$\{\}$	Column vector.

*Address all correspondence to this author.

INTRODUCTION

Performance optimization is an essential goal aimed by helicopter manufacturers to enhance their machines. Naturally, blade design is an important research topic, targeting better lift capabilities, noise reductions or vibratory comfort for both passengers and pilots. Such improvements lead to design composite blades with curved shapes and important twist characteristics. At the predesign stage, 3D models cannot be used regarding for meshing issues, calculation time and parametric studies. That is why many efforts have been and are still done in the field of beam elastic modeling.

Early researches [1–3] introduced successively twist effects, coupling between bending and torsion motions and coupling terms due to gravity and shear center non coincidence. Initially curved beams have been investigated in [4–6]. Librescu and Song [7] treat the problem using thin walled beam theories applied to composite blades. For more complicated beams, twist dependency, geometrical non-linearity and rotational effects have to be introduced properly in both kinetic and strain energies before applying Hamilton's principle to derive the equations of motion. The reference work in the field of helicopter blade modeling using this so-called "exact" method has been brought by Hodges [8] who produced numerous publications on this topic among them a survey paper [9] and the reference book [10]. His work has been widely used since then for composite blade modeling [11], cross-sectional characteristics calculation [12, 13], and comprehensive analysis codes assessment [14].

Numerically speaking, elastic beam modeling is split up in two independent parts: a 2D problem which lead to compute cross-sectional mass and stiffness characteristics, and a 1D problem for solving the equations of motion. In this research the first problem is considered as a prerequisite, providing necessary data input for the proposed beam model. Characteristics are computed using [15] investigations on composite blade with arbitrary cross-sections. Developments made by [16–18] introduced a whole strain matrix able to properly reduce the initial 3D problem with a high level of reliability.

The Finite Element Method is a very convenient way to solve the equations of motion (e.g. to solve the remaining 1D problem), both for static purpose and dynamic analysis. Batoz and Dhatt [19] give a global overview of beam finite element modeling and one can refer to Lalanne and Ferraris [20] for rotating issues applied to turbomachinery.

A highly accurate finite element based on Hermite's functions has been developed to increase convergence speed and avoiding shear locking effect as shown in [21]. Besides, to improve the modeling of the complex coupling between torsion and bending motions, Timoshenko's shear coefficient [22–24] has been introduced in every matrices of the mechanical system, including geometrical stiffness matrix and centrifugal force work. Criesfield work [25] on the co-rotational formulation has been used to provide to the highly accurate finite element the large deflection compliance required by hinged rotor blade modeling. It is worth noticing here that equations of motion have been derived in the rotational frame, in order to catch all rotatory effects in the element definition.

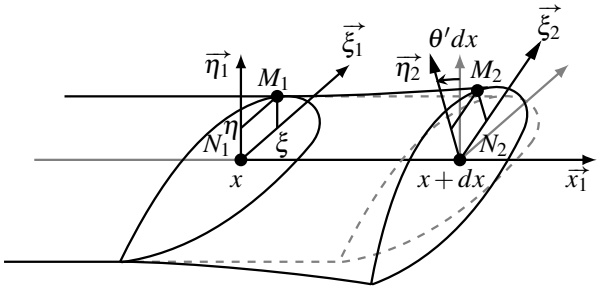

FIGURE 1. LENGTH OF AN UNDEFORMED FIBER

A brief theoretical recall of the equations of motion developped in this research is given, emphasizing the geometrical non-linearity of the strain field and the introduction of shear effects. Then, the specific 1D Finite Element formulated gathers efficiently in a new consistent Beam Advanced Model all the effects encountered by a composite rotating blade with arbitrary cross-sections and shapes. At last numerical and experimental results are provided to illustrate the model capacities.

THEORY

By assumption the neutral fiber is taken as the reference axis. The pure torsion motion is considered as independent from bending, longitudinal and coupling induced torsion motions and is applied separately. A second order approximation scheme is used to derive non-linear equations of motion. Lagrange's equations are recalled here as they constitute a very common way to determine equations of motion using Hamilton's principle applied to strain and kinetic energies. The conservative and homogeneous equations of motion are given by:

$$\frac{\partial}{\partial t}\left(\frac{\partial T}{\partial \dot{q}_i}\right) - \frac{\partial T}{\partial q_i} + \frac{\partial U}{\partial q_i} = 0 \tag{1}$$

Beam strain field

The dimensional reduction introduced by beam theories results in the limitation of the strain field to fibers axial elongation (and to the cross-section torsion angle). For initially curved beam one has to consider only a short piece of the beam, with a length dx, considered as straight. For twisted beam, with a twist angle per unit length of θ', the fiber length calculation is illustrated in Fig. 1. The length of an unspecified fiber M_1M_2 is then:

$$\left|\overrightarrow{M_1M_2}\right| = \left(1 + \frac{1}{2}(\eta^2 + \xi^2)\theta'^2\right) dx \tag{2}$$

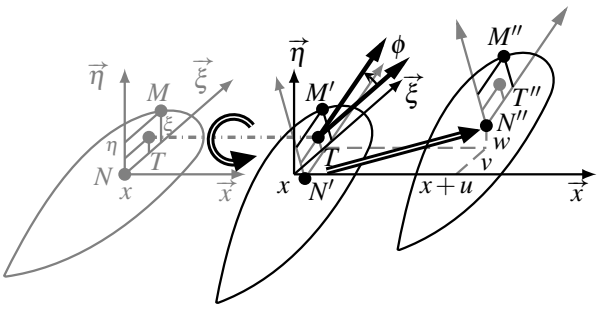

FIGURE 2. DECOMPOSITION OF BEAM DEFORMATION

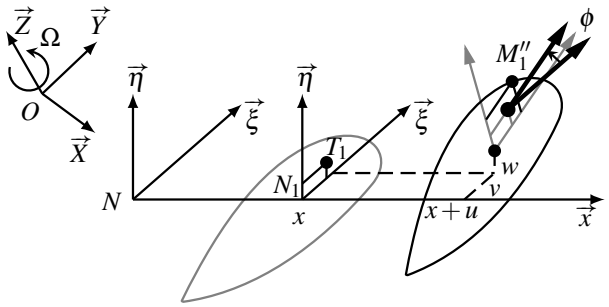

FIGURE 3. CROSS-SECTION DISPLACEMENT FIELD

The initial R frame, defined by its origin N and its leading axes $\vec{x}$, $\vec{\xi}$ and $\vec{\eta}$, is used to describe the displacement field of one of the beam cross-section (Fig. 2). The cross-section motion is applied in two steps: first it undergoes the torsion motion represented by a twist angle ϕ around the shear center T, then the elastic center N is moved by longitudinal motion u and bending motions v and w.

Considering a point M of the initial cross-section, M' is its counterpart after torsion motion and M'' its counterpart after bending and axial motions. M and T are simply linked by their coordinates in initial R frame respectively $\langle 0, \xi, \eta \rangle$ and $\langle 0, \xi_t, \eta_t \rangle$. M' an T are linked in the twisted frame by the same relation which is rotated by the angle ϕ when expressed in R frame.

Introducing small bending angles ϕ_ξ around $\vec{\xi}$ and ϕ_η around $\vec{\eta}$, one can retrieve the link between M' and M'' with $\eta_{M'}$ and $\xi_{M'}$ the coordinates of M' in R frame.

$$\overrightarrow{M'M''} = \left\{ \begin{array}{c} u + \eta_{M'}\phi_\xi - \xi_{M'}\phi_\eta \\ v - \xi_{M'}\dfrac{\phi_\eta^2}{2} \\ w - \eta_{M'}\dfrac{\phi_\xi^2}{2} \end{array} \right\}_R \tag{3}$$

The length of the fiber M_1M_2 after all motions being applied to cross-sections can be deduced by decomposing the vector $\overrightarrow{M_1''M_2''}$.

$$\begin{aligned} \overrightarrow{M_1''M_2''} = {} & \overrightarrow{M_1''M_1'} + \overrightarrow{M_1'T_1} + \overrightarrow{T_1M_1} \\ & + \overrightarrow{M_1M_2} \\ & + \overrightarrow{M_2T_2} + \overrightarrow{T_2M_2'} + \overrightarrow{M_2'M_2''} \end{aligned} \tag{4}$$

$$\varepsilon = \frac{\left|\overrightarrow{M_1''M_2''}\right| - \left|\overrightarrow{M_1M_2}\right|}{\left|\overrightarrow{M_1M_2}\right|} \tag{5}$$

All calculations achieved, one can write the strain field of a cross-section, with linear and non-linear parts containing coupling terms between each of the motions. k and h are two constants independent from motion parameters.

$$\varepsilon_l = u' - \xi\phi_\eta' + \eta\phi_\xi' + k\theta'\phi' \tag{6}$$

$$\begin{aligned} \varepsilon_{nl} = {} & \frac{u'^2}{2} + \frac{v'^2}{2} + \frac{w'^2}{2} + \frac{\phi_\eta^2}{2}\eta^2\theta'^2 + \frac{\phi_\xi^2}{2}\xi^2\theta'^2 + h\phi'^2 \\ & + \xi^2\frac{\phi_\eta'^2}{2} + \eta^2\frac{\phi_\xi'^2}{2} + (\xi - \xi_t)x\phi_\xi'\phi' \\ & + (\eta - \eta_t)x\phi_\eta'\phi' + \xi\theta'u'\phi_\xi + \eta\theta'u'\phi_\eta + \eta u'\phi_\xi' \\ & - \xi u'\phi_\eta' + \xi\eta\theta'\phi_\xi\phi_\xi' - \xi\eta\theta'\phi_\eta\phi_\eta' + \xi\eta\theta'^2\phi_\xi\phi_\eta \\ & - \xi\eta\phi_\xi'\phi_\eta' - \xi^2\theta'\phi_\eta'\phi_\xi + \eta^2\theta'\phi_\eta\phi_\xi' \end{aligned} \tag{7}$$

Timoshenko's beam theory permits to link bending angles and lateral displacements :

$$\phi_\eta = v' + C_\xi \quad , \quad \phi_\xi = -w' + C_\eta \tag{8} \quad , \quad (9)$$

Beam velocity field

The fixed frame R_0 is defined by O, $\vec{X}$, $\vec{Y}$ and $\vec{Z}$ in Fig. 3. The speed of rotation of the beam around $\vec{Z}$ is Ω. Point O coordinates in R frame is $\langle x_A, \xi_A, \eta_A \rangle$. Using Eqn. (3), one can find the position of a point M_1 after application of the displacement field.

$$\overrightarrow{OM_1''} = \overrightarrow{ON} + \overrightarrow{NN_1} + \overrightarrow{N_1T_1} + \overrightarrow{T_1M_1'} + \overrightarrow{M_1'M_1''} \tag{10}$$

$$\overrightarrow{OM_1''} = \left\{ \begin{array}{c} x_A + x + u + (\eta + (\xi - \xi_t)\phi)\,\phi_\xi - (\xi - (\eta - \eta_t)\phi)\,\phi_\eta \\ \xi_A + \xi\left(1 - \dfrac{\phi_\eta^2}{2}\right) + v - (\eta - \eta_t)\phi \\ \eta_A + \eta\left(1 - \dfrac{\phi_\xi^2}{2}\right) + w + (\xi - \xi_t)\phi \end{array} \right\}_R \tag{11}$$

Introducing $\overrightarrow{\Omega_{R_1/R_0}}$ the rotational vector expressed in R frame, the velocity of point M_1 is then :

$$\overrightarrow{V_{M_1}} = \frac{\partial \overrightarrow{OM_1''}}{\partial t} + \overrightarrow{\Omega_{R_1/R_0}} \wedge \overrightarrow{OM_1''} \tag{12}$$

$$\frac{\partial \overrightarrow{OM_1''}}{\partial t} = \begin{Bmatrix} \dot{u} + \eta\dot{\phi}_\xi - \xi\dot{\phi}_\eta \\ \dot{v} - (\eta - \eta_t)\dot{\phi} \\ \dot{w} + (\xi - \xi_t)\dot{\phi} \end{Bmatrix}_R \tag{13}$$

$$\overrightarrow{\Omega_{R_1/R_0}} = \begin{Bmatrix} \Omega_1 \\ \Omega_2 \\ \Omega_3 \end{Bmatrix}_R \tag{14}$$

Kinetic energy

Kinetic energy is directly calculated from the velocity field along the beam :

$$T = \frac{1}{2}\int_V \rho V_M^2 dV \tag{15}$$

Kinetic energy terms can be gathered depending on their order and their derivation with respect to time. 2nd order "velocity" terms lead to define a mass matrix. The stiffness matrix can be obtained with 2nd order "displacement" terms, while cross products between velocity and displacement terms make appear the gyroscopic matrix. At last first order "displacement" terms correspond to centrifugal force work. Other terms disappear when Lagrange's equations are applied.

$$T = T_{mass} + T_{stiff} + T_{gyro} + T_{cf} + T_{other} \tag{16}$$

Strain energy

The total strain energy is the sum of the pure torsion strain energy resulting from the angle of torsion ϕ around the shear center T and characterized by the torsion constant J_T, and of the strain energy due to fibers elongation.

$$U = U_T + U_S \tag{17}$$

$$U_T = \frac{1}{2}\int_L G J_T \phi'^2 dx \tag{18}$$

$$U_S = \frac{1}{2}\int_V E\varepsilon^2 dV \tag{19}$$

As the strain field can be decomposed in a linear and a non-linear part, both shear dependent (Eqns. (8) (9) in (6) (7)), the resulting strain energy should be divided as well :

$$U_S = U_{lin} + U_{nl} + U_{ho} + U_{shear} \tag{20}$$

The classical linear strain energy comes from linear terms cross-products:

$$U_{lin} = \frac{1}{2}\int_V E\varepsilon_l^2 dV \tag{21}$$

The effects of the initial stress σ_0 are brought by non-linear terms. Resulting strain energy is responsible for the stress stiffening of the beam.

$$U_{nl} = \int_V E\varepsilon_l\varepsilon_{nl} dV = \int_V \sigma_0\varepsilon_{nl} dV \tag{22}$$

The part of strain field coming from transverse shear (Eqns. (24) (25)) produces a shear energy which is directly linked to Timoshenko's beam theory and its shear coefficients k_ξ and k_η for each bending axis :

$$U_{shear} = \frac{1}{2}\int_V (2\sigma_{x\xi}\varepsilon_{x\xi} + 2\sigma_{x\eta}\varepsilon_{x\eta}) dV \tag{23}$$

$$2\varepsilon_{x\xi} = -\phi_\eta + v' \quad , \quad 2\varepsilon_{x\eta} = \phi_\xi + w' \tag{24) , (25}$$

$$\frac{T_\xi^2}{k_\xi S} = \int \sigma_{x\xi} dS \quad , \quad \frac{T_\eta^2}{k_\eta S} = \int \sigma_{x\eta} dS \tag{26) , (27}$$

with T_ξ and T_η the transverse forces applied to the cross-section and S its area. kS represents the equivalent sheared area also often called "reduced section".

Writing transverse shear stresses one can finally obtain the shear energy.

$$\sigma_{x\xi} = 2Gk_\xi\varepsilon_{x\xi} \quad , \quad \sigma_{x\eta} = 2Gk_\eta\varepsilon_{x\eta} \tag{28) , (29}$$

$$U_{shear} = \frac{1}{2}\int_V 4G(k_\xi\varepsilon_{x\xi}^2 + k_\eta\varepsilon_{x\eta}^2) dV \tag{30}$$

Remaining high order terms U_{ho} can be neglected regarding to the approximation scheme.

Equations of motion

Introducing results from Eqns. (16) and (17) in Eqn. (1) the final equations of motion governing the rotating beam movements can be formed.

$$M\ddot{q} + C(\Omega)\dot{q} + \left(K + K_G(\sigma_0) - K_S(\Omega^2)\right) q = F_C(\Omega^2) + F_{ext} \tag{31}$$

Conveniently the matrix form of the equations makes appear classical mass matrix M, including rotatory inertia, and stiffness matrix K, including shear and torsion stiffness. C is the gyroscopic matrix responsible for the Coriolis Effect acting on ro-

tating beams. Two additional stiffness matrices are defined: K_G is the stress stiffening matrix due to centrifugal load, K_S is the spin softening matrix that counteracts K_G in the rotating frame to equilibrate the stiffness of the beam. F_C and F_{ext} are respectively the centrifugal forces vector and the external forces vector applied to the beam.

FINITE ELEMENT APPROACH

A Beam Advanced Model (BAM) is proposed in this paper based on a highly accurate finite element. This element has to minimize the number of DoF needed for a whole blade model since it will have to fit into a comprehensive rotorcraft analysis code in a second step of the model development. It takes properly into account shear effects avoiding though the shear locking numerical phenomena. It has some non-classical DoF for a higher accuracy and is fully compliant with numerical methods requirements of articulated rotor such as the co-rotational formulation [25]. Moreover this element is devoted to rotational frame studies in which vibrations of helicopter blades occur.

Formulation of the finite element

The choice of shape functions is one of the main issues when formulating a FE, conditioning DoF that will be included in the model, accuracy of the results and complexity of the model.

In order to respect the equilibrium equations in the case of axial and torsion motions, the BAM FE has to keep different the nodal slopes of two adjacent FE. Consequently using such a FE requires to have 10 DoF at each node (Fig. 4). However it should be mentioned that another solution consists in using a cubic isoparametric FE composed of four nodes having each the classical 6 DoF. Such a FE permits modeling a step-section beam with the same accuracy, but increases the number of nodes making the numbering delicate to manage. The first approach is retained because the numerical implementation is easier to carry out and the number of DoF required is lower.

For lateral displacements, classical cubical shape functions are chosen in order to link corresponding bending angles. The BAM FE requires also cubical shape functions for longitudinal displacement and for torsion motion.

$$u(x) = a_1 + a_2 x + a_3 x^2 + a_4 x^3 \tag{32}$$
$$v(x) = a_5 + a_6 x + a_7 x^2 + a_8 x^3 \tag{33}$$
$$w(x) = a_9 + a_{10} x + a_{11} x^2 + a_{12} x^3 \tag{34}$$
$$\phi(x) = a_{13} + a_{14} x + a_{15} x^2 + a_{16} x^3 \tag{35}$$

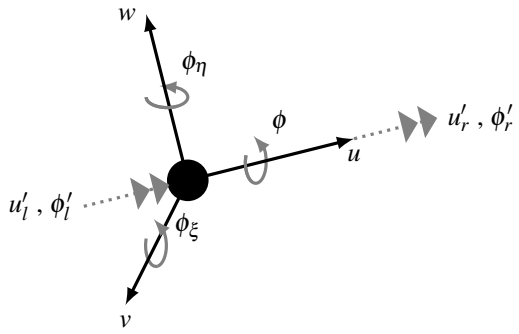

FIGURE 4. BAM DEGREES OF FREEDOM FOR ONE NODE

Nodal displacements and their slopes constitute the DoF of the FE. They are related to shape functions by boundary conditions. First 6 DoF are classical 3D beam DoF used to locate and orientate each node in space. The 4 remaining DoF are the derivatives of longitudinal displacement and torsion angle coming from left-side element and right-side element (resp. l and r subscripts). Each node has to separate their contributions. The BAM FE is then related to 20 DoF.

$$\begin{aligned}\langle \delta_N \rangle = \langle & u_1, v_1, w_1, \phi_1, \phi_{\xi 1}, \phi_{\eta 1}, u'_{1l}, u'_{1r}, \phi'_{1l}, \phi'_{1r}, \\ & u_2, v_2, w_2, \phi_2, \phi_{\xi 2}, \phi_{\eta 2}, u'_{2l}, u'_{2r}, \phi'_{2l}, \phi'_{2r} \rangle\end{aligned} \tag{36}$$

Coefficients of Eqns. (32) and (35) are easily found using element boundary conditions for longitudinal and torsion motions (Eqns. (37) to (40)) . For bending motions, shear effects have to be added in order to correctly derive shape functions coefficients. This step is described in a dedicated section.

$$u(0) = u_1 \quad , \quad u(L) = u_2 \tag{37}$$
$$u'(0) = u'_{1r} \quad , \quad u(L) = u'_{2l} \tag{38}$$
$$\phi(0) = \phi_1 \quad , \quad \phi(L) = \phi_2 \tag{39}$$
$$\phi'(0) = \phi'_{1r} \quad , \quad \phi(L) = \phi'_{2l} \tag{40}$$

Highly accurate beam element

Shape functions (32) to (35) are linear compositions of Hermite's cubical functions (see Fig. 5) which involve the derivatives of each motion in the overall description of the beam elastic behavior. This is the case in particular for the nodal slopes of longitudinal and torsion motions. The interest is to be able to let them free when connecting two beam elements, and doing so to ensure torque and axial load transmission between two elements with different cross-sectional characteristics, with no need for a mesh refinement around the transition zone. The accuracy of the beam model is then highly increased for composite blades with a axial-torsion-bending coupled behavior.

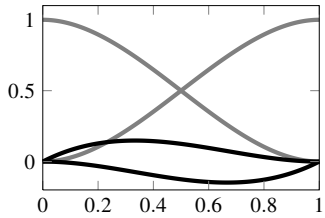

FIGURE 5. HERMITE'S CUBICAL FUNCTIONS

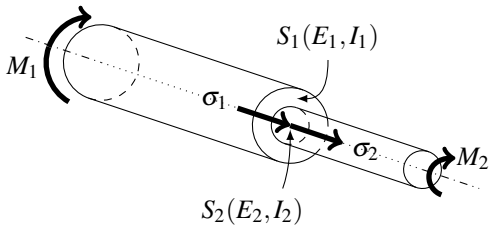

FIGURE 6. TORQUE AND AXIAL LOAD TRANSMISSION

The demonstration of the advantages of the BAM FE is quite simple. Fig. 6 illustrates torque and axial load (resp. M and σ) transmission between two cylindrical elements with different radius and made of two different materials. Strength of material laws give Eqns. (41) to (44).

$$M_1 = E_1 I_1 \frac{\partial \phi_1}{\partial x} \quad , \quad M_2 = E_2 I_2 \frac{\partial \phi_2}{\partial x} \qquad (41)\ ,\ (42)$$

$$\sigma_1 = \frac{E_1}{S_1}\frac{\partial u_1}{\partial x} \quad , \quad \sigma_2 = \frac{E_2}{S_2}\frac{\partial u_2}{\partial x} \qquad (43)\ ,\ (44)$$

Torque and longitudinal load are to be transmitted from element 1 to element 2. It is assumed that $E_1 I_1 \neq E_2 I_2$ and $\frac{E_1}{S_1} \neq \frac{E_2}{S_2}$. This implies that the derivatives of longitudinal and torsion motions on each side of the common node are not equal.

$$\frac{\partial u_1}{\partial x} \neq \frac{\partial u_2}{\partial x} \quad , \quad \frac{\partial \phi_1}{\partial x} \neq \frac{\partial \phi_2}{\partial x} \qquad (45)\ ,\ (46)$$

In Standard Beam FE (SdB) with linear shape functions and 6 DoF per node, these derivatives can not be included in the formulation. To get the same range of accuracy when performing a clamped-free dynamic analysis looking for torsion and longitudinal modes, one must use much more elements with a SdB model.

Table 1 gives some results for the two cylinders example. Reference results are obtained using a high number of beam elements, both BAM and SdB converging toward this solution.

Cylinders characteristics : Length $L_1 = L_2 = 1m$, Radius $r_1 = 0.1m$ and $r_2 = 0.05m$, Material characteristics $E_1 = 2.10^{11}N$ and $E_2 = 7.10^{10}N$, $\rho_1 = 7800Kg.m^{-3}$ and $\rho_2 = 2000Kg.m^{-3}$.

TABLE 1. FREQUENCIES OF FIRST MODES OF THE TWO CYLINDERS EXAMPLE

Mode type	Bend. 1	Bend. 2	Tors. 1	Tors. 2	Longi. 1
Ref. results	*70.7197*	*147.419*	*752.791*	*949.289*	*1117.99*
SdB 2 elem. 12 DoF	71.0376 (0.450%)	148.458 (0.705%)	819.160 (8.816%)	1062.49 (11.92%)	1196.71 (7.041%)
SdB 10 elem. 60 DoF	70.7223 (0.004%)	147.445 (0.017%)	755.4836 (0.358%)	953.787 (0.474%)	1121.19 (0.286%)
BAM 2 elem. 20 DoF	71.0392 (0.452%)	148.465 (0.709%)	752.826 (0.005%)	949.395 (0.011%)	1118.02 (0.002%)
BAM 4 elem. 40 DoF	70.7573 (0.053%)	147.657 (0.161%)	752.792 (0.000%)	949.290 (0.000%)	1117.99 (0.000%)

These results clearly show the benefits of BAM for torsion and longitudinal modes. With only 2 elements (the minimum number of elements required for this problem) BAM is right on the reference results while SdB is far from the converged solution. It is worth noticing that accuracy for bending modes is almost the same for the two models. Looking for an acceptable solution with SdB (e.g. less than 0.5% of relative error) 10 elements are needed. Increasing the accuracy for BAM on bending modes requires 4 elements. Finally, less DoF are needed with BAM to get the same range of accuracy on any kind of mode.

Shear locking free element

Transverse shear effects modify the beam behavior in bending motions, adding cross-section rotations to ones produced by lateral displacements. In Timoshenko's theory lateral displacements and bending angles are kinematically linked together trough Eqns. (8) and (9). This relation between bending motions parameters can be translated numerically by the field consistence approach (see [21]).

Focusing on only one bending motion, Fig. 7 exhibits how forces and momentum are balanced within a short piece of beam. Equations (24), (26) and (28) can be combined to retrieve the classical relation between the shear transverse force T and the supplementary shear rotation angle C_ξ.

$$T = C_\xi k_\xi SG \qquad (47)$$

Static equilibrium and strength of material laws give the following relations:

$$\frac{\partial T}{\partial x} = 0 \quad , \quad \frac{\partial M}{\partial x} = T \qquad (48)\ ,\ (49)$$

$$\frac{\partial \phi_\eta}{\partial x} = \frac{M}{EI} \qquad (50)$$

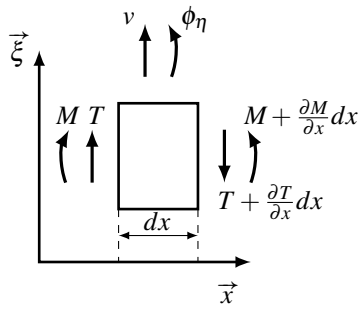

FIGURE 7. BEAM EQUILIBRIUM

Deriving Eqn. (8) gives:

$$\frac{\partial^2 \phi_\eta}{\partial x^2} = \frac{\partial^3 v}{\partial x^3} \tag{51}$$

Eventually Eqns. (47) to (51) permit to link the shear coefficient k_ξ and the shear rotation angle:

$$C_\xi = \frac{EI}{k_\xi G}\frac{\partial^3 v}{\partial x^3} \tag{52}$$

As for longitudinal displacement and torsion angle, shape function coefficients are deduced from boundary conditions at element nodes, Eqns. (53) and (54).

$$v(0) = v_1 \quad , \quad v(L) = v_2 \tag{53}$$

$$\phi_\eta(0) = \phi_{\eta 1} \quad , \phi_\eta(L) = \phi_{\eta 2} \tag{54}$$

Deriving the shape function gives:

$$\frac{\partial v}{\partial x} = a_6 + 2a_7 x + 3a_8 x^2 = \phi_\eta - C_\xi \tag{55}$$

$$\frac{\partial^3 v}{\partial x^3} = 6a_8 \tag{56}$$

Using $a_\xi = \dfrac{12EI}{GK_\xi SL^2}$ the shear coefficient introduced by [26], one can finally link the shear rotation angle with the shape function coefficients. The shear coefficient a_ξ is conveniently almost null for long slender beams for which shear effects can be neglected, and ensures to retrieve a classical Euler-Bernoulli model in this case, without shear locking effect.

$$C_\xi = \frac{L^2 a_\xi}{2} a_8 \tag{57}$$

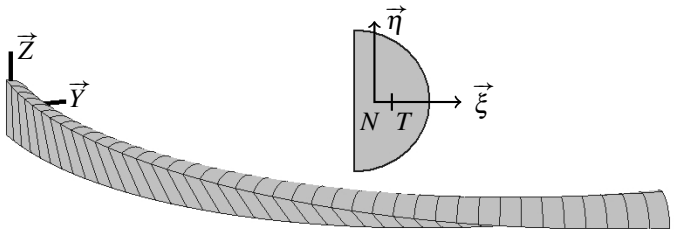

FIGURE 8. TWISTED AND CURVED BEAM

VALIDATION OF BAM

The BAM FE is implemented in MATLAB to assess its capabilities. Model validation is based on both numerical and experimental investigations.

Numerical validation

The assessment of the BAM FE has to be methodical in order to validate separately all the assumptions that were made and to investigate all non-classical effects encountered by complex beams. In this scope some academic test beams were defined specifically for this purpose. One of the most interesting beams is a highly twisted homogeneous curved beam with a semi-disc cross-section (Fig. 8). This beam is clamped-free, rotating around its $\vec{Z}$ axis at a Ω speed of rotation.

Beam characteristics : Length $L = 1m$, Diameter $d = 70mm$, Twist angle at tip $\theta = 90$, Material characteristics $E = 2\ 10^{11}Pa$, $\nu = 0.3$, $\rho = 7800kg.m^{-3}$, Shear coefficients $ky = 0.766$ $kz = 0.863$, Torsion constant $J_T = 4.46\ 10^{-7}m^4$.

TABLE 2. NATURAL FREQUENCIES OF THE 10 FIRST MODES AT $\Omega = 100rad.s^{-1}$

Mode Type	InP 1	OuP 1	InP 2	OuP 2	InP 3
SOLID186	*29.6596*	*45.3156*	*160.809*	*201.843*	*504.470*
BEAM44	28.9249 (-2.48%)	44.6130 (-1.55%)	157.071 (-2.32%)	200.120 (-0.85%)	494.204 (-2.04%)
BAM	28.7738 (-3.02%)	44.8059 (-1.12%)	158.077 (-1.70%)	202.662 (0.41%)	497.045 (-1.47%)
Mode Type	OuP 3	InP 4	OuP 4	InP 5	OuP 5
SOLID186	*609.725*	*914.543*	*1031.72*	*1230.98*	*1662.65*
BEAM44	601.261 (-1.65%)	906.615 (-0.87%)	1010.01 (-2.10%)	1212.09 (-1.53%)	1647.14 (-0.93%)
BAM	601.261 (-1.39%)	905.701 (-0.97%)	1017.94 (-1.34%)	1211.01 (-1.62%)	1657.16 (-0.33%)

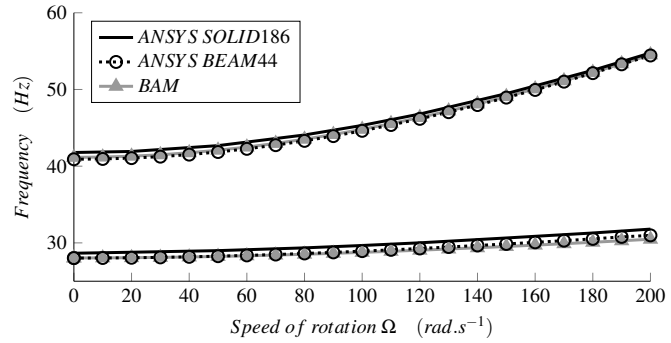

FIGURE 9. CAMPBELL DIAGRAM OF THE 2 FIRST MODES

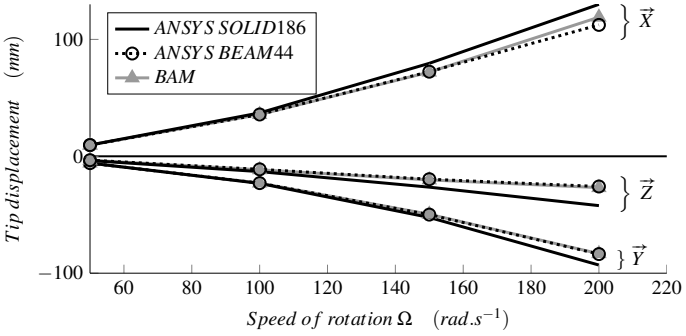

FIGURE 10. TIP DISPLACEMENT UNDER CENTRIFUGAL LOADS

Reference results are coming from a ANSYS 3D model made of 6400 SOLID186 elements. SOLID186 element is a hexagonal element with 20 nodes, 6 DoF per node. Two 1D models are compared: BAM (40 elements) and an ANSYS BEAM44 model (40 elements). BEAM44 is a 3D beam element with 2 nodes, 6 DoF per node, compliant with arbitrary cross-sections and rotating frame.

Table 2 presents the 10 first natural frequencies at $\Omega = 100 rad.s^{-1}$. Figure 9 is a Campbell diagram for the first two modes up to $200 rad.s^{-1}$. Modes are named whether they have a deformed shape mainly in the XY plane (InP) or out of this plane (OuP).
Correlation between reference 3D model results and BAM is very satisfying. Frequency results keep in the range of $\pm 3\%$ for the ten first modes. Mode shapes, not represented here, are also well computed. BAM and BEAM44 have comparable accuracy ranges as torsion motion is not dominant in mode shapes. However this comparison permits to validate the good behavior of BAM FE on a tricky test case.

Another interesting result is the tip displacement under centrifugal loads. Displacements for $\vec{X}$, $\vec{Y}$ and $\vec{Z}$ directions are represented in Fig. 10. It is very important to correctly compute those displacements both for pure static analysis and for stress stiffening computation which modifies significantly the dynamic behavior of the beam. Again BAM and BEAM44 results are very close. Both beam models slightly underestimate the tip displacement, and doing so underestimate the axial stress and the resulting stiffening of the beam. This statement can be seen in Tab. 2 noticing that frequencies are slightly below the ones computed with the 3D model.

All those results show that BAM is well suited for curved and twisted rotating beams. In the case of actual helicopter blades, the model encounters an aerodynamic load field in addition to centrifugal loads. Moreover it has to take into account the composite cross-section. However this test case is quite representative of the BAM FE ability to model complex shaped blades, with a very good range of accuracy.

Experimental validation

The experimental assessment of BAM is scheduled on the Eurocopter Blue Edge^{TM} blade which has a very specific double swept plan shape (Fig. 11) optimized for acoustic and performance. This blade takes advantage of a new composite structure for fatigue and resistance, and of innovative aerodynamic features including an increase of the twist angle along the span. It gathers all the modeling issues the BAM FE has been designed for. Only normalized results are available in accordance with Eurocopter confidentiality policy.

Impulsive tests The first tests performed with the Blue Edge^{TM} blade are impulsive tests for modal characterization. The blade is hung by sandows to ensure "pseudo" free-free boundary conditions. Measurement equipment is compound of 11 accelerometers distributed span wise, on the leading edge, on the trailing edge and on the 25% chord axis. The natural modes are excited with an impact hammer. The free-free dynamic analysis is achieved with BAM. Normalized natural frequencies are presented in Tab. 3 and first normalized deformed shapes in Fig. 12.

This assessment has to be analyzed from a qualitative point

TABLE 3. NORMALIZED FREQUENCIES OF FIRST FREE-FREE MODES

Mode type	Mode 1	Mode 2	Mode 3	Mode 4	Mode 5
Exp. results	*1.000*	*3.26*	*5.81*	*6.01*	*11.74*
BAM	0.998 (-0.23%)	3.29 (0.89%)	5.56 (-4.25%)	6.03 (0.31%)	11.90 (1.29%)

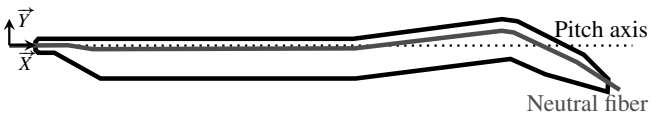

FIGURE 11. BLUE EDGE^{TM} BLADE

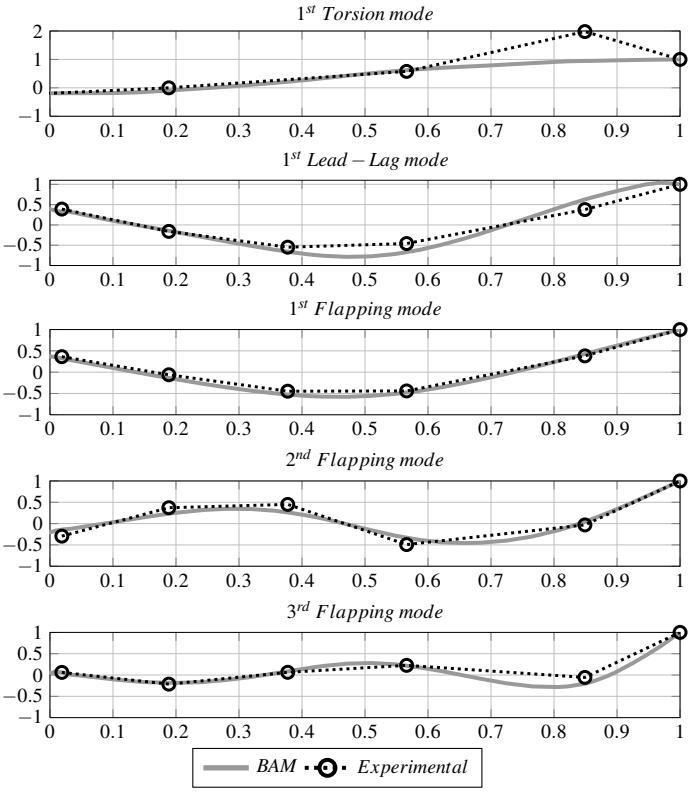

FIGURE 12. NORMALIZED FIRST NATURAL MODE SHAPES

of view since two major issues are encountered. First one is the difficulty to catch properly the global deformation of the blade experimentally. Only projected deformed shapes are available, coupling between motions is not measured. Second issue deals with the position of the shear center which depends on the boundary conditions. This position is slightly moved whether clamped-free conditions (as when mounted on a rotor hub) or free-free conditions are used. Anyway, these tests are important to assess the model for dynamic purpose in the worst conditions.

From Tab. 3, it can be shown that BAM is not too far from measurements, emphasizing the fact that the overall characteristics of the blade are well represented. Figure 12 illustrates the good prediction of the projected deformed shapes, even if the first torsion mode seems to be difficult to apprehend. Those results illustrates the robustness of BAM and its ability to model with efficiency the dynamic of swept blades.

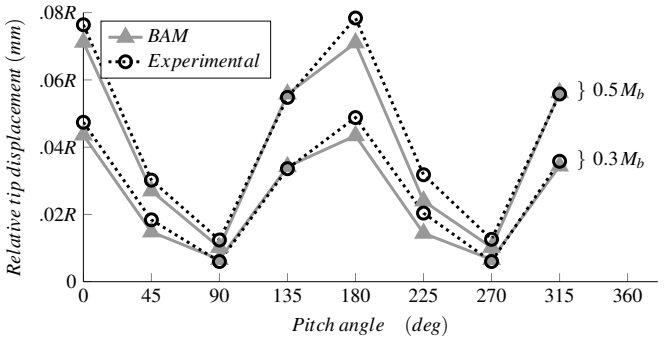

FIGURE 13. TIP DISPLACEMENT VS. PITCH ANGLE

Bending test The second experimental test performed is a bending test at rest, looking for tip displacement. The blade is rigidly attached on a test bench by its root. The test bench is driven in term of pitch angle. For each pitch angle a reference position is measured while the blade is bending under its own weight M_b. Then an additional mass is hung at 90% of the radius R, and the relative tip displacement is measured. Two different masses were used. A synthesis of the results are presented in Fig. 13.

The global results are very satisfying, demonstrating a good level of prediction of the bended shapes with BAM. The static calculation of the deformation of a blade is essential when coupling an elastic model to an aerodynamic code since the flow field is highly influenced by the blade position. Even if those results should be deepened and extended to torsion motion, they emphasize the accuracy of BAM when large deflections are needed as it is the case here, with a relative tip displacement close to 10% of the blade radius. One can notice the slight differences between two opposite positions of the blade. This is due to the non-homogeneity of cross-sections. Some material non-linearities could also explain the increase of the variation between BAM and experimental results at a pitch angle close to $200deg$. However since the stiffness of a rotating beam is mainly driven by its stress stiffening, this error should vanish for a whirl tower test.

CONCLUSION

Beam theories have been studied for a long time. Though, they can be enhanced for some specific applications which require modeling non-classical effects such as rotational effects, shear effects or non-linear geometric effects. In the field of helicopter blade modeling this research aimed to design a new beam FE with a high level of accuracy. Enhancements were provided both for the establishment of the equations of motion and for the FE formulation.

Numerical investigations were performed to assess the FE. The test beam with emphasized characteristics compared to an actual blade has exhibited a very good behavior of the Beam Advanced Model FE, and a good accuracy both on mode shapes and frequencies. First experimental results are provided to assess the representativeness of the model for an actual blade design such as the Eurocopter Blue Edge^{TM} blade. Some extended results, including whirl tower test, will be discussed in a further paper.

ACKNOWLEDGMENT

The authors would like to acknoweledge Eurocopter for the support and data provided during this research.

REFERENCES

[1] Montoya, J., 1966. "Vibrations couplées de flexion et torsion d'une aube vrillée en rotation". *Revue Brown Boveri,* ***53***(3), pp. 216 – 230.

[2] Isakson, G., and Eisley, J. G., 1964. Natural frequencies in coupled bending and torsion of twisted rotating blades. Tech. rep., NASA. CR 65, NSG 27-59.

[3] Ferraris, G., 1982. "Prévision du comportement dynamique des ensembles disque-aubes". PhD thesis, INSA de Lyon. 126p., ITC3 8202.

[4] Bauchau, O. A., and Hong, C. H., 1987. "Large displacement analysis of naturally curved and twisted composite beams". *AIAA Journal,* ***25***, Nov., pp. 1469 – 1475.

[5] Borri, M., Ghiringhelli, G. L., and Merlini, T., 1992. "Linear analysis of naturally curved and twisted anisotropic beams". *Composites Engineering,* ***2***(5-7), pp. 433 – 456.

[6] Petrov, E., and Géradin, M., 1998. "Finite element theory for curved and twisted beams based on exact solutions for three-dimensional solids part 1: Beam concept and geometrically exact nonlinear formulation". *Computer Methods in Applied Mechanics and Engineering,* ***165***(1-4), pp. 43 – 92.

[7] Librescu, L., and Song, O., 2006. *Thin-Walled composite beam*. Springer.

[8] Hodges, D., and Dowell, E., 1974. Nonlinear equations of motion for the elastic bending and torsion of twisted nonuniform rotor blade. Tech. rep., NASA. Number: A-5711, NASA-TN-D-7818.

[9] Hodges, D. H., 1990. "Review of composite rotor blade modeling". *AIAA Journal,* ***28***, Mar., pp. 561–565.

[10] Hodges, D., 2006. *Nonlinear composite beam theory*. Progress in astronautics and aeronautics. American Institute of Aeronautics and Astronautics.

[11] Yu, W., Hodges, D. H., Volovoi, V., and Cesnik, C. E. S., 2002. "On timoshenko-like modeling of initially curved and twisted composite beams". *International Journal of Solids and Structures,* ***39***(19), pp. 5101 – 5121.

[12] Cesnik, C. E. S., Hodges, D. H., and Sutyrin, V. G., 1996. "Cross-sectional analysis of composite beams including large initial twist and curvature effects". *AIAA Journal,* ***34***, Sept., pp. 1913–1920.

[13] Friedmann, P. P., Glaz, B., and Palacios, R., 2009. "A moderate deflection composite helicopter rotor blade model with an improved cross-sectional analysis". *International Journal of Solids and Structures,* ***46***(10), pp. 2186 – 2200.

[14] Volovoi, V. V., Hodges, D. H., Cesnik, C. E. S., and Popescu, B., 2001. "Assessment of beam modeling methods for rotor blade applications". *Mathematical and Computer Modelling,* ***33***(10-11), pp. 1099 – 1112.

[15] Puspita, G., 1993. "Conception assisté par ordinateur de poutre composites (application aux pales d'hélicoptère)". PhD thesis, SUPAERO Toulouse. 344p., 93 ESAE 0018.

[16] Puspita, G., Barrau, J. J., and Gay, D., 1993. "Computation of flexural and torsional homogeneous properties and stresses in composite beams with orthotropic phases". *Composite Structures,* ***24***(1), pp. 43 – 49.

[17] Sudre, M., and Barrau, J.-J., 1996. "Determination du tenseur complet des contraintes dans des poutres composites". In *Journées nationales sur les composites N° 10*.

[18] Taufik, A., Barrau, J. J., and Lorin, F., 1999. "Composite beam analysis with arbitrary cross section". *Composite Structures,* ***44***(2-3), pp. 189 – 194.

[19] Batoz, J., and Dhatt, G., 1992. *Modélisation des structures par éléments finis*, Vol. 1-3. Presses de l'Université Laval, 2763772528.

[20] Lalanne, M., and Ferraris, G., 1998. *Rotordynamics prediction in engineering*, 2nd ed. John Wiley.

[21] Yunhua, L., 1998. "Explanation and elimination of shear locking and membrane locking with field consistence approach". *Computer Methods in Applied Mechanics and Engineering,* ***162***(1-4), pp. 249 – 269.

[22] Timoshenko, S., 1934. *Theory of elasticity*. Engineering societies monographs. McGraw-Hill book company, inc.

[23] Cowper, G. R., 1966. "The shear coefficient in timoshenko's beam theory". *Journal of Applied Mechanics*.

[24] Hutchinson, J. R., 2001. "Shear Coefficients for Timoshenko Beam Theory". *Journal of Applied Mechanics,* ***68***(1), pp. 87 – 92.

[25] Crisfield, M., 1997. *Non-linear finite element analysis of solids and structures*, Vol. 2. Wiley.

[26] Przemieniecki, J., 1985. *Theory of matrix structural analysis*. Dover books on engineering. Dover. ISBN : 0-486-64948-2.